

# Obesity resistance of the stearoyl-CoA desaturase-deficient (*scd1*<sup>-/-</sup>) mouse results from disruption of the epidermal lipid barrier and adaptive thermoregulation

Erika Binczek<sup>1</sup>, Britta Jenke<sup>1</sup>, Barbara Holz<sup>1</sup>, Robert Heinz Günter<sup>1</sup>, Mario Thevis<sup>2</sup> and Wilhelm Stoffel<sup>1,\*</sup>

<sup>1</sup>Laboratory of Molecular Neurosciences, Center of Molecular Medicine (CMMC), Center of Biochemistry, Faculty of Medicine, University of Cologne, Joseph-Stelzmann-Str. 52, D-50931 Köln, Germany

<sup>2</sup>Institut für Biochemie, DSHS Köln, D-50933 Köln, Germany

\*Corresponding author

e-mail: wilhelm.stoffel@uni-koeln.de

## Abstract

Targeted deletion of the stearoyl-CoA desaturase 1 gene (*scd1*) in mouse causes obesity resistance and a severe skin phenotype. Here, we demonstrate that SCD1 deficiency disrupts the epidermal lipid barrier and leads to uncontrolled transepidermal water loss, breakdown of adaptive thermoregulation and cold resistance, as well as a metabolic wasting syndrome. The loss of  $\omega$ -hydroxylated very long-chain fatty acids (VLCFA) and ceramides substituted with  $\omega$ -hydroxylated VLCFA covalently linked to corneocyte surface proteins leads to the disruption of the epidermal lipid barrier in *scd1*<sup>-/-</sup> mutants. Artificial occlusion of the skin by topical lipid application largely reconstituted the epidermal barrier and also reversed dysregulation of thermogenesis and cold resistance, as well as the metabolic disturbances. Interestingly, SCD1 deficiency abolished expression of the key transcription factor Lef1, which is essential for interfollicular epidermis, sebaceous glands, and hair follicle development. Finally, the occurrence of SCD1 and a newly described *hSCD5* (*ACOD4*) gene in humans suggests that the *scd1*<sup>-/-</sup> mouse mutant might be a valuable animal model for the study of human skin diseases associated with epidermal barrier defects.

**Keywords:** dysregulation of thermogenesis; epidermal lipid barrier breakdown; hypermetabolism; obesity resistance; SCD1 deficiency; VLCFA synthesis.

## Introduction

A key enzyme of mammalian lipid metabolism is stearoyl-CoA desaturase (SCD; EC 1.14.99.5), which desaturates *de novo* synthesized palmitoyl- and stearoyl-CoA to palmitoleic ( $\Delta 9$ -16:1) and oleic acid ( $\Delta 9$ -18:1), essential components of triglycerides and complex lipids in lipoproteins and eukaryotic membranes. SCD1 is part of a trimeric complex consisting of the subunits desaturase, cytb5, and NADH-cytb5 reductase, which is integrated in

the membrane of the endoplasmic reticulum and stereospecifically introduces a single  $\Delta 9$ -*cis* double bond. Four genes encode the stearoyl-CoA desaturase isoforms (SCD1–4) in the mouse and at least two *scd* loci (*Scd1* and *Scd4*) are known in man (Kaestner et al., 1989; Miyazaki et al., 2003; Ntambi et al., 2004; Dobrzyn and Ntambi, 2005). *Scd1* and *Scd3* are expressed predominantly in liver, sebaceous glands of the skin, and the Meibomian glands of the eyelid, *Scd2* in brain, and *Scd4* exclusively in heart muscle (Miyazaki et al., 2001).

The first insights into systemic and tissue-specific functions of SCD came from two spontaneous autosomal recessive mutants of the mouse *scd1* locus, *asebia*<sup>J</sup> (*ab*<sup>J</sup>) (Zheng et al., 1999) and *asebia*<sup>2J</sup> (*as*<sup>2J</sup>) (Sundberg et al., 2000; Miyazaki et al., 2001). They share strong phenotypic similarities with *scd1*<sup>-/-</sup> mouse mutants generated by gene targeting described here and previously. Repression of monounsaturated fatty acid and lipoprotein syntheses in liver has been postulated to be the root cause of hypermetabolism and obesity resistance causing a reduction in adipose tissue, both defining features of SCD1 deficiency (Cohen et al., 2002, 2003; Cohen and Friedman, 2004). A recent micro-array expression study to unravel the metabolic response of leptin-regulated genes in leptin-treated *ob/ob* mice revealed reduced hepatic *scd1* gene expression. The lack of obesity found in the *ob/ob* mouse was ameliorated in the double mutant *ob/ob ab*<sup>J</sup>/*ab*<sup>J</sup>. This finding led to the conclusion that *scd1* is a target of leptin in the liver (Sundberg et al., 2000). The other main phenotypic markers are severe skin lesions with atrophy of sebaceous glands of the epidermis, Meibomian glands of the eyelid, and disturbed hair growth. However, to date, a conclusive molecular interpretation of the basic mechanism underlying obesity resistance (leanness) and the link to the severe skin phenotype of *scd1*<sup>-/-</sup> mutants remain elusive.

In this study we address the question as to whether repression of monounsaturated fatty acid and lipoprotein syntheses in liver or breakdown of the epidermal lipid barrier plays the primary role in the development of SCD1 deficiency phenotype. Here, we demonstrate that the structural basis for the severe skin pathology observed in *scd1*<sup>-/-</sup> mice is due to a lack of the covalently linked ceramide brushborder-like matrix, the basis of the epidermal lipid barrier breakdown.

## Results

### Generation of *scd1*-null mice

The *scd1* gene was disrupted in CJ7-ES cells by homologous recombination using a replacement vector containing the genomic sequence of exons I–IV, in which exon II was disrupted by a *neo*-gene cassette (Figure

1A–C). G418 and gancyclovir-resistant ES cell clones that carried the targeted allele were used to generate chimeric male mice that passed the mutant *scd1* allele to their offspring. Southern blot analysis of *StuI*-restricted DNA from ES cell clones and mouse-tail genomic DNA allowed detection of the homologous recombination event in the *scd1* locus. The steady-state mRNA concentrations of *scd1*, *scd2*, and *scd3* in liver and skin, as well as in brain and kidney, were determined by semi-quantitative RT-PCR (Figure 1E), which revealed the absence of *scd1* and tissue-specific expression of *scd2* and *scd3*. Furthermore, the loss of SCD1 activity in the liver microsomal fraction of null mice (data not shown) demonstrated that we had successfully inactivated the *scd1* gene. Wild-type, heterozygous, and homozygous offspring were obtained in the expected Mendelian ratio. *scd1*<sup>-/-</sup> mice were viable and fertile.

### Parameters of lipid metabolism in SCD1-deficient mice

Serum lipid parameters in metabolically unchallenged control and *scd1*<sup>-/-</sup> mice differed only marginally. Serum

triglyceride concentration in VLDL was 135±30 mg/dl in wild-type and 110±35 mg/dl in *scd1*<sup>-/-</sup> mice (n=5), while total cholesterol was 66±5 mg/dl in control mice versus 75±6 mg/dl in *scd1*<sup>-/-</sup> mice (n=10 each). Serum cholesterol was only slightly elevated.

No significant quantitative differences among ester and amide lipid classes in total lipid extracts of liver, brain, and kidney from control and *scd1*<sup>-/-</sup> mice were found by HPTLC and densitometric quantification (data not shown). However, GC-MS analysis of methyl esters of the fatty acyl residues indicated that the saturation index (18:0/18:1) was considerably elevated in liver and skin, but not in brain of the *scd1*<sup>-/-</sup> mouse (Figure 1F). The absence of palmitoleate (16:1) in liver, skin, and brain of *scd1*<sup>-/-</sup> mice is most remarkable. In contrast, oleic acid was still present, most likely due to the redundant desaturase isoenzymes SCD2, SCD3, and SCD4. To examine this further, SCD1-deficient and control mice were kept for 2 months on a fat-free diet and the 16:0/16:1 and 18:0/18:1 ratios were subsequently determined by GLC of fatty acids of total lipid extracts of liver. Identical patterns of liver fatty acids for mice fed *ad libitum* on a

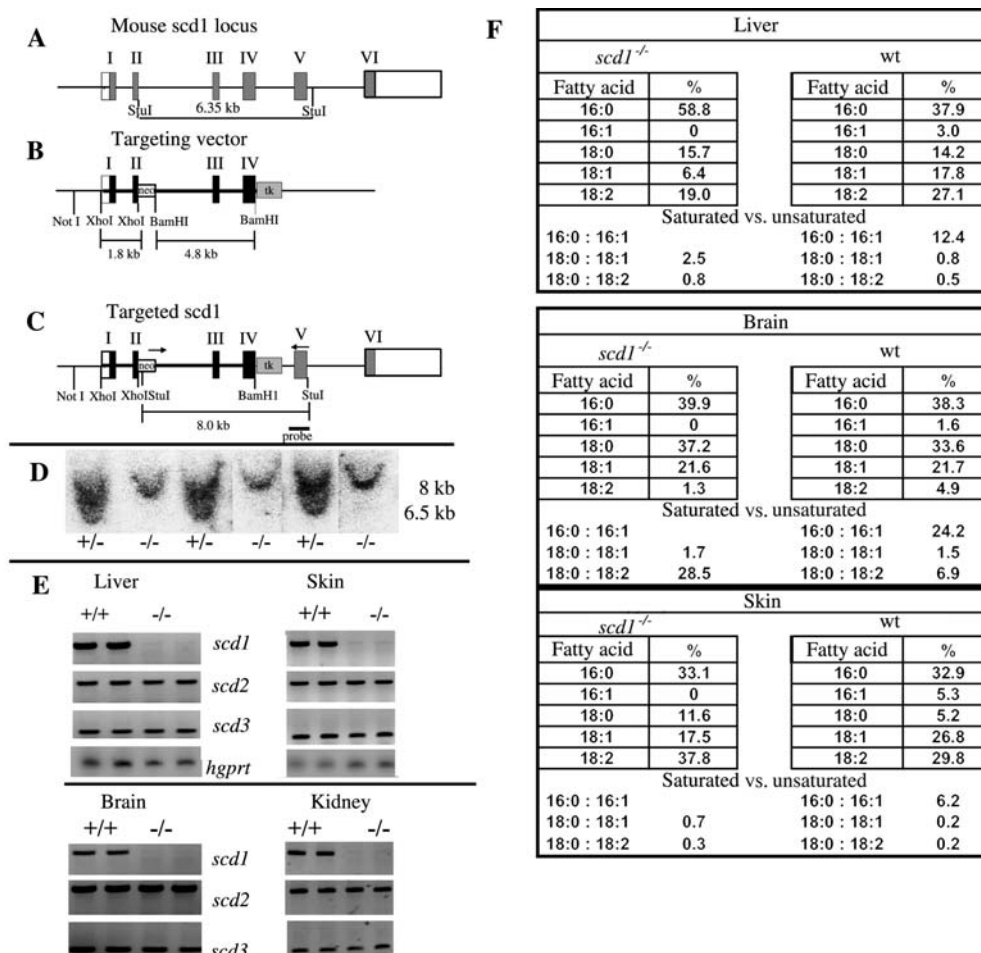


**Figure 1** Strategy for targeted disruption of the murine *scd1* gene in ES cells.

Disruption of the *scd1* gene by homologous recombination. (A) Mouse wt *scd1* locus with *StuI* restriction fragment of 6.35 kb. (B) Targeting vector consisting of a 1.8-kb *XhoI* fragment with exons I and II and a 4.8-kb *BamHI* fragment harboring exons III and IV. (C) Targeted *scd1* locus with an 8.0-kb *StuI* RFLP and location of the 3' external probe and PCR primers (neo-sense and exon V antisense). (D) Southern blot analysis of genomic DNA of a selected *StuI*-restricted, G418-resistant ES cell clone (lane 1) and of mouse tail genomic DNA (lanes 2–6). (E) Steady-state mRNA concentrations of *scd1*, *scd2*, and *scd3* in liver, skin, brain, and kidney: semi-quantitative RT-PCR. (F) Increased ratio of saturated to unsaturated fatty acids in total lipids of liver, brain and skin. Quantitative analysis of fatty acid methyl esters by GC.

fat-free diet strongly indicated that the oleic acid remaining in liver, skin, and brain was synthesized by isoenzymes SCD2 and SCD3. In addition, the daily oral application of 20 mg of palmitoleic and oleic acids to newborn wild-type and *scd1*<sup>-/-</sup> mice failed to change the fatty acid pattern of liver lipids or to rescue the phenotype (data not shown).

### Metabolic wasting syndrome in the *scd1*<sup>-/-</sup> mouse

Loss of adipose tissue (leanness) in the *scd1*<sup>-/-</sup> mouse may result from restricted food intake or enhanced energy expenditure. SCD1-deficient mice rapidly lost their subcutaneous, interscapular, mesenteric, and epididymal fat pads, despite free food access (Figure 2A). We

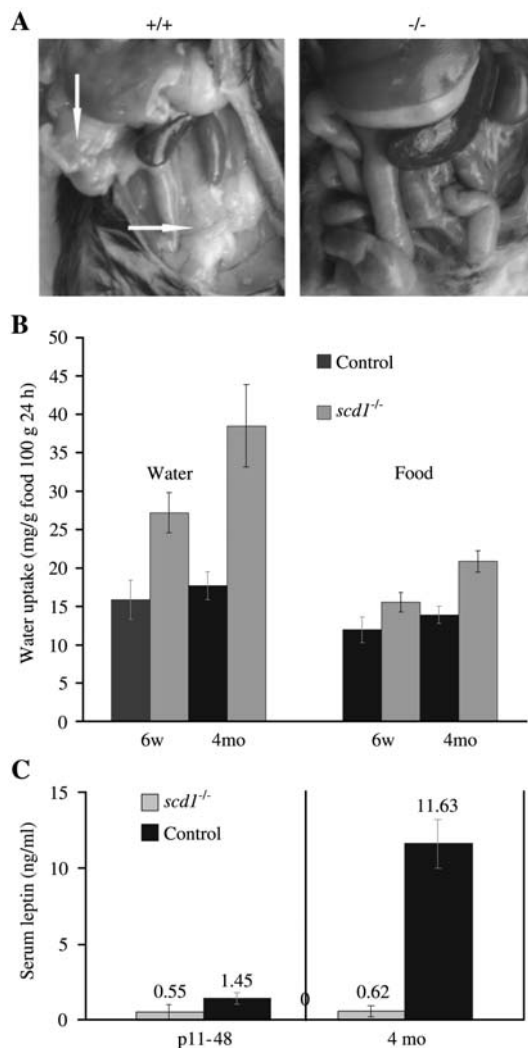


**Figure 2** Depletion of fat depots (leanness) and increased water and food uptake in the *scd1*<sup>-/-</sup> mouse. (A) *scd1*<sup>-/-</sup> mice (4 months old) lost their visible visceral, inguinal and subcutaneous fat stores. (B) SCD1-deficient mice have increased water and food uptake. Cohorts (n=8) of p42 and p120 male wt and *scd1*<sup>-/-</sup> mice were housed in metabolic cages with free food and water access for 5 days. Food uptake in the *scd1*<sup>-/-</sup> mice was 33±8% and 43±8% higher and water uptake 93±6% and 145±5%, respectively, than in control cohorts (p<0.001). (C) Serum leptin concentrations, quantified by immunoassay, were strongly reduced: 18-fold in 4 months and three-fold in p11-p48 *scd1*<sup>-/-</sup> mice compared with control mice (cohorts n=5 each).

compared food and water uptake in wild-type and *scd1*<sup>-/-</sup> mice (n=8 each) at 6 weeks and 4 months of age. Food uptake in *scd1*<sup>-/-</sup> mice was 33±8% and 43±8% higher and water uptake 93±6% and 145±5%, respectively, than in control cohorts (p<0.001) (Figure 2B).

The role of the adipocyte hormone leptin in the regulation of energy homeostasis is well known and documented in the obesity (*ob/ob*) mouse mutant with deficient leptin expression (Friedman and Halaas, 1998). Crossing the *scd1*<sup>-/-</sup> locus into *ob/ob* transferred the phenotypic characteristics of hypermetabolism and reduction of adipose tissue in the double mutant *ob/ob*×*scd1*<sup>-/-</sup> and ameliorated the obese phenotype. It has been suggested that SCD1 deficiency mimics the rescue of leptin function in the *ob/ob* mouse. From these observations, the conclusion was drawn that SCD1 is an important metabolic control point in leptin signaling (Cohen and Friedman, 2004).

Serum leptin concentrations in cohorts (n=5) of our *scd1*<sup>-/-</sup> mice and wild-type mice at weaning age were 0.55±0.1 and 1.45±0.25 ng/ml, and 0.62±0.2 and 11.63±2.6 ng/ml, respectively, in adult mice (Figure 2C). Therefore, we conclude that the strong reduction in serum leptin concentration is secondary to the loss of adipose tissue.

### The epidermal lipid barrier is disrupted

We next focused our analysis on the properties of the perturbed epidermal lipid barrier of *scd1*<sup>-/-</sup> mice. We measured three parameters that probed the integrity of the epidermal lipid barrier functions: transepidermal water loss (TEWL) *in vivo* (Figure 3A), transdermal passive transport of the water-soluble solute [<sup>3</sup>H]-mannitol *in vitro* (Figure 3B), and penetration of the fluorescent dye Lucifer yellow *in vivo* (Figure 3C). TEWL was quantified in areas of the front and back skin of cohorts of 10 gender- and age-matched control and *scd1*<sup>-/-</sup> mice at different ages. Independent of the site of the measurement, TEWL was three- to four-fold higher (25–28 g/h m<sup>2</sup> ±5) in adult (2 months) *scd1*<sup>-/-</sup> mice (n=25) than in control cohorts (8–9 g/h m<sup>2</sup> ±4, n=25) (Figure 3A) (p<0.001). Skin of p20 postnatal, wild-type and *scd1*<sup>-/-</sup> mice became permeable in both directions, outside-in and inside-out. Permeability was assessed using [<sup>3</sup>H]-mannitol as an uncharged solute. The diffusion of [<sup>3</sup>H]-mannitol through the isolated skin of age and gender matched wild-type and *scd1* null mice was measured in a two-chamber system. The intact epidermal lipid barrier of postnatal day 14 (p14) and p48 control mice prohibited the outside-in diffusion of Lucifer yellow through the skin *in vivo*, but the fluorescent dye diffused deeply into the dermis of *scd1*<sup>-/-</sup> mice, as shown in the fluorescence images of Figure 3C.

### Failure of adaptive thermoregulation in *scd1*<sup>-/-</sup> mice

The permanently elevated TEWL in the *scd1*<sup>-/-</sup> mouse requires enhanced fuel oxidation for heat production to maintain temperature homeostasis, which puts severe stress on energy homeostasis in this mutant mouse. Temperature homeostasis is controlled in mammals at the sites of brown (BAT) and white adipose tissue (WAT), as well as in muscle. We conducted quantitative indirect

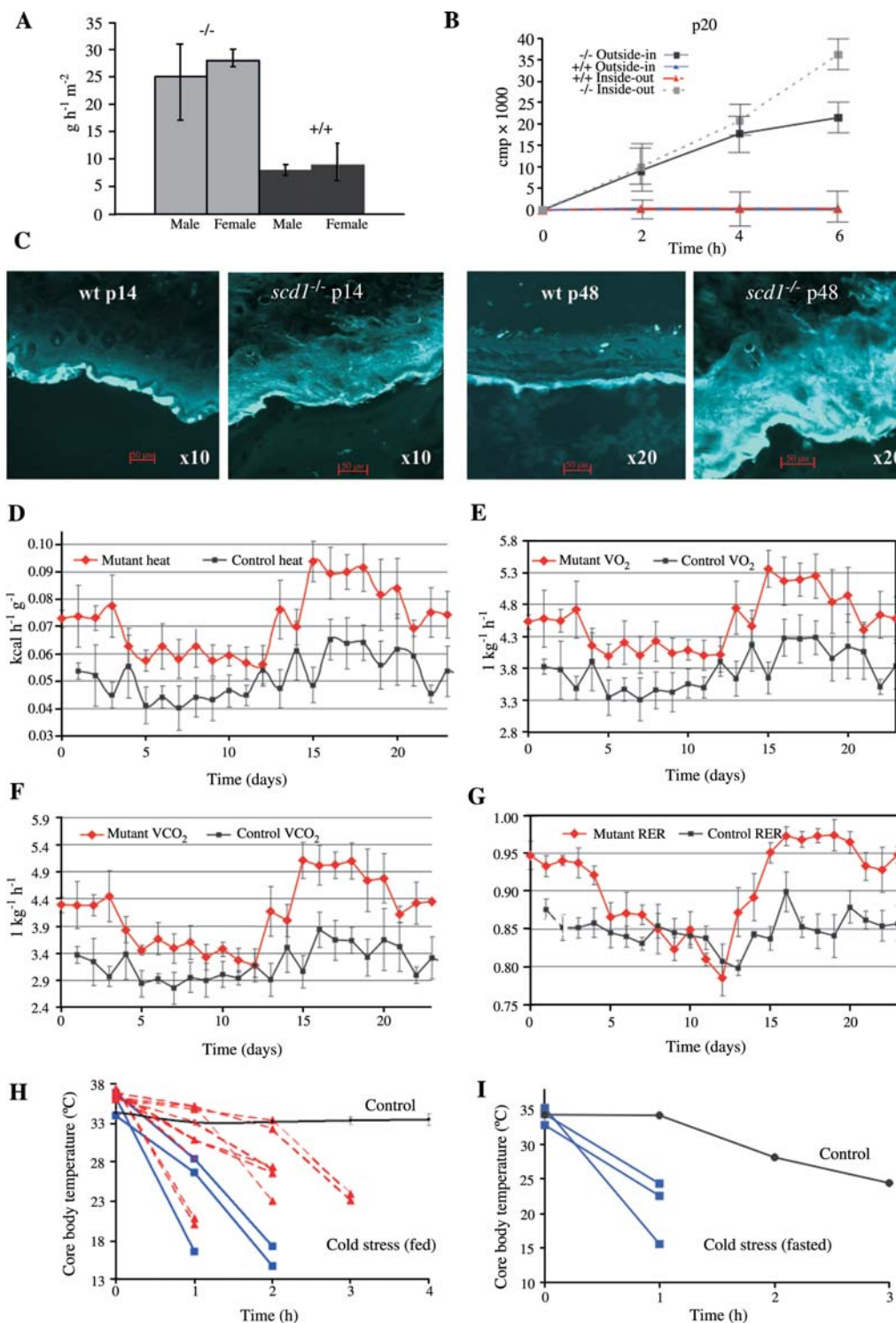


**Figure 3** Disrupted epidermal barrier function causes elevated transepidermal water loss (TEWL), enhanced permeability, elevated heat dissipation, hypermetabolism and breakdown of thermoregulation in the cold stress experiment. (A) TEWL of gender-matched cohorts (n=5) of wild-type control and *scd1*<sup>-/-</sup> mice. (B) *In vitro* inside-out and outside-in diffusion of [<sup>3</sup>H] mannitol through skin excised from p20 wild-type and *scd1*<sup>-/-</sup> mice in the two-chamber system. (C) Fluorescence micrographs show the penetration of Lucifer yellow into p14 and p48 wild-type and *scd1*<sup>-/-</sup> back skin *in vivo*. Indirect calorimetry of gender-matched controls and *scd1*<sup>-/-</sup> littermates indicated excess heat loss, and increased O<sub>2</sub> consumption and CO<sub>2</sub> production in *scd1*<sup>-/-</sup> mice during the photo- and scotophases. (D) Heat dissipation (kcal h<sup>-1</sup> kg<sup>-1</sup>). (E) O<sub>2</sub> consumption (l/h kg). (F) CO<sub>2</sub> production (l/h kg). (G) RER (respiratory ratio); controls, solid black line; *scd1*<sup>-/-</sup>, red line (n=6); error bars denote SE. Breakdown of thermoregulation in *scd1*<sup>-/-</sup> mice. Core body temperature during cold stress at 4°C for wild-type (n=6) and *scd1*<sup>-/-</sup> mice: 1 month (n=3) and 3 months (n=8) for (H) fed mice and (I) fasting mice.

calorimetry over a period of 24 h with cohorts of control and *scd1*<sup>-/-</sup> mice at the ambient temperature of 23°C, which is 7°C below thermoneutrality. *scd1*<sup>-/-</sup> mice showed significant heat loss (Figure 3D) and increased O<sub>2</sub> consumption and CO<sub>2</sub> production during scotophase, which was even stronger during photophase (Figure 3E,F). The respiratory quotient (RER, CO<sub>2</sub> exhaled/O<sub>2</sub> consumed) in adult *scd1*<sup>-/-</sup> mice was considerably higher than that of the control animals, indicating a switch to glucose oxidation as the source for energy production in the absence of fat depots (Figure 3G).

### Loss of adaptive thermoregulation in SCD1-deficient mice causes fatal cold stress

*scd1*<sup>-/-</sup> and control mice (p48) rapidly became cold-intolerant when the ambient temperature was shifted from 23°C to 4°C. The core body temperature of SCD1-deficient animals with free access to food dropped from 36.6±1°C to at least 27°C within 2–3 h, resulting in death due to cold stress within 4 h. In contrast, control mice maintained a core body-temperature balance between 36.6±0.5°C and 33±0.5°C during the 48-h period in which they were subjected to cold stress (Figure 3H). When the 4°C cold stress experiment was performed under fasting conditions after an overnight fast at 23°C, the core body temperature of *scd1*<sup>-/-</sup> mice decreased by at least 10°C within 1–2 h, but in wild-type mice this took between 3 and 6 h to occur (Figure 3I).

Despite free access to food and elevated phosphoenolpyruvate carboxykinase (*pepck*) expression in liver of *scd1*<sup>-/-</sup> mice, indicating enhanced gluconeogenesis, serum glucose in *scd1*<sup>-/-</sup> mice decreased during cold stress from 110–120 to <50–60 mg/dl, whereas serum glucose in control mice remained around 85–110 mg/dl.

### Adaptive thermogenesis in *scd1* null mice

Adaptive thermogenesis is regulated largely by the activation of uncoupling protein UCP1 in the inner mitochondrial membrane of BAT and muscle. Transcriptional coactivators of nuclear receptors, PGC1α and β, play an important role in *ucp1* expression (Puigserver et al., 1998). We investigated the expression of these key factors in relation to adaptive thermogenesis in *scd1*<sup>-/-</sup> mice, and observed dramatic changes in the expression of *ucp1*, *pgc1α* and *pgc1β* in BAT and muscle (Figure 4A–E). In BAT, expression levels of *pgc1α* was strongly (14-fold) reduced in *scd1*<sup>-/-</sup> compared to control mice, and expression of *ucp1* and *ucp3* was hardly measurable in *scd1*<sup>-/-</sup> mice. Steady-state mRNA levels of *ucp1*, *ucp2*, and *ucp3* in skeletal muscle of *scd1*<sup>-/-</sup> mice at 23°C were increased 16-, 1.2-, and 1.5-fold, respectively, compared to wild-type littermates, whereas *pgc1α* and *pgc1β* expression remained unchanged. These observations suggest that skeletal muscle is an important energy donor in adaptive thermogenesis in the *scd1*<sup>-/-</sup> mouse.

### Rescue of epidermal barrier functions by topical paraffin occlusion of the skin of *scd1* null mice

To further verify our conclusion that breakdown of the epidermal lipid barrier and excessive TEWL are respon-

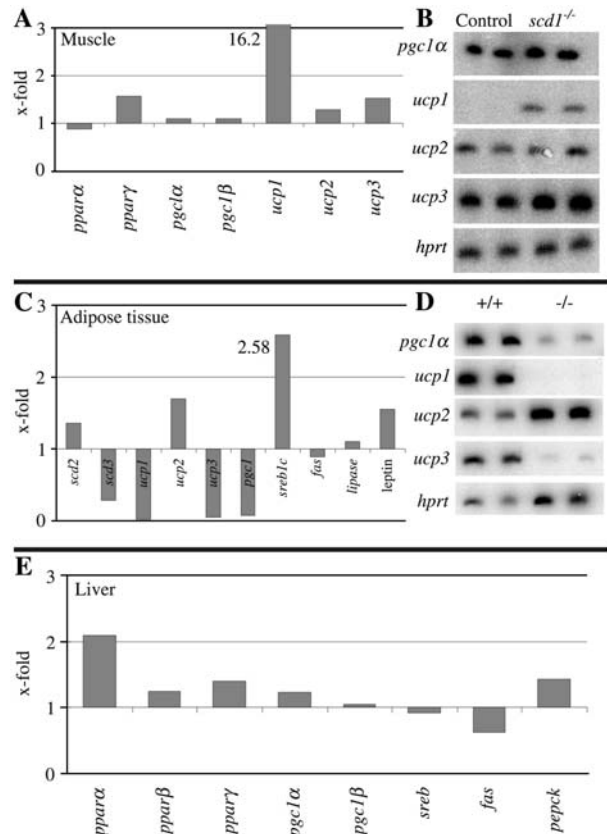


**Figure 4** Steady-state mRNA levels of genes regulating adaptive thermogenesis in muscle, brown adipose tissue and liver at 23°C.

(A) Muscle *pparα*, *pparγ*, *pgc1α* and *pgc1β*, *ucp1*, *ucp2* and *ucp3*. (B) Steady-state levels of mRNA of *pgc1α*, *ucp1*, *ucp2* and *ucp3*. (C) Brown adipose tissue: *scd2*, *scd3*, *ucp1*, *ucp2*, *ucp3*, *pgc1α*, *sreb1c*, *fas*, *lipase*, and *leptin*. (D) Steady-state levels of mRNA of *pgc1α*, *ucp1*, *ucp2* and *ucp3*. (E) Liver: *pparα*, *pparβ*, *pparγ*, *pgc1α*, *pgc1β*, *sreb1c*, *fas*, and *pepck*. (B) and (D) are representative examples of auto-radiochromatograms of labeled cDNA fragments obtained by RT-PCR of muscle (B) and adipose tissue (D) mRNA with *hpri* for normalization of signals. RNA was isolated from pooled tissues of five male controls and five *scd1*<sup>-/-</sup> mice, aged 6 weeks.

sible for the hypermetabolic parameters (O<sub>2</sub> consumption, CO<sub>2</sub> production, heat dissipation, and the fatal cold stress of *scd1*<sup>-/-</sup> mice), we tried to reverse the abnormalities of the permeability barrier function by occluding the skin using topical application of petrolatum Vaseline. This artificial barrier dramatically improved the negative impact of the metabolic disturbances. The excessively high TEWL (Figure 5A) and heat loss (Figure 5B) were reversed by approximately half, temperature resistance in the cold stress experiment was rescued, and the metabolic rate [O<sub>2</sub> consumption (Figure 5C), CO<sub>2</sub> production (Figure 5D), and RER (Figure 5E)] improved in *scd1*<sup>-/-</sup> mice.

The artificial hydrocarbon barrier normalized the response to cold stress. The drop in core body temperature was parallel to that observed in wild-type siblings within 5 h (Figure 5F).

Serum glucose and insulin concentrations, ketone bodies, glucose tolerance test, serum-free fatty acids, LDL, HDL, total cholesterol and triglyceride concentra-

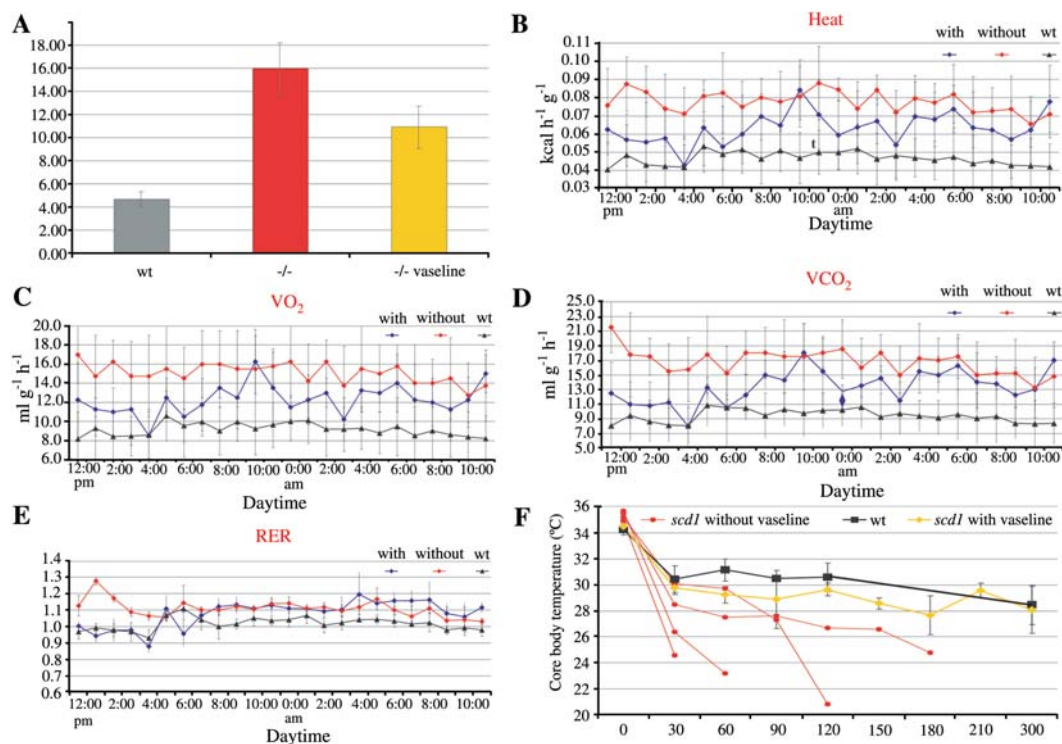


**Figure 5** Rescue of metabolic parameters of *scd1*<sup>-/-</sup> mice coated with paraffin.

(A) Transepidermal water loss (TEWL) of 8-week-old gender-matched cohorts (n=4) of wt (gray bar), *scd1*<sup>-/-</sup> (red bar), and *scd1*<sup>-/-</sup> coated with Vaseline (yellow bar). Indirect calorimetry of gender-matched *scd1*<sup>-/-</sup> and *scd1*<sup>-/-</sup> littermates coated with Vaseline indicated excess heat loss, as well as increased O<sub>2</sub> consumption and CO<sub>2</sub> production, in SCD1-deficient mice during both photo- and scotophases. (B) Heat dissipation (kcal h<sup>-1</sup> kg<sup>-1</sup>). (C) O<sub>2</sub> consumption (ml h<sup>-1</sup> kg<sup>-1</sup>). (D) CO<sub>2</sub> production (ml h<sup>-1</sup> kg<sup>-1</sup>). (E) RER (respiratory ratio). Controls, black line; *scd1*<sup>-/-</sup>, red line (n=6); error bars denote SE. (F) Recovery of thermoregulation in *scd1*<sup>-/-</sup> mice. Core body temperature during cold stress at 4°C of wild-type (n=4) (black line), untreated *scd1*<sup>-/-</sup> mice (n=4) (red lines), and *scd1*<sup>-/-</sup> mice coated with vaseline (n=4) (yellow line).

tions of Vaseline-coated *scd1*<sup>-/-</sup> mice matched those of the control animals (data not shown).

### The epidermis-specific, surface-bound ceramide envelope is missing in *scd1*<sup>-/-</sup> mice

We next investigated the molecular basis of the impaired epidermal intercorneocytic lipid barrier. Epidermis and dermis of p1 and p2 control and *scd1*<sup>-/-</sup> mice were separated for the analysis of freely extractable lipids and those covalently bound to corneocytes. Epidermis from wild-type and *scd1*<sup>-/-</sup> mice contained phosphatidylcholine and phosphatidylethanolamine only as minor components. Sphingomyelin and glucosyl ceramide, the two precursors of skin ceramides, together with free fatty acids, ceramides, and cholesterol represented the main components of the extractable lipid fraction in the epidermis (Figure 6A).

$\omega$ -Hydroxy-ceramides are linked via an ester bond to surface proteins of stratum granulosum/stratum corneum keratinocytes (Wertz and Downing, 1986). We released protein-bound lipids from extensively extracted epidermis by mild alkaline treatment. Separation and identification of the total lipid extract by HPTLC revealed that the epidermis-specific ceramide fraction was almost absent in the *scd1*<sup>-/-</sup> mouse, while traces of cholesterol and other unsaponifiable substances were still present (Figure 6B). This fraction was then cleaved by acid methanolysis and  $\omega$ -hydroxy-fatty acid methyl esters

were derivatized by trimethylsilylation for GC-MS analysis and quantification (Figure 6C,D).

The alkali-labile, protein-bound ceramide fraction of control mice contains the epidermis-specific VLCFA. More than two-thirds of the fatty acyl residues present in protein-bound ceramides of control mice were  $\omega$ -hydroxy-VLCFA C30:0,  $\omega$ -OH-C32:0,  $\omega$ -OH-C34:0, and  $\omega$ -OH-C32:1. On the other hand, *scd1*<sup>-/-</sup> epidermis contained only minor amounts of VLCFA, approximately 5–7% of total fatty acids. These findings correlate well with the results for gene expression of enzymes participating in the microsomal chain elongation complex and  $\omega$ -hydroxylation of VLCFA in the skin (Figure 7A): ELOVL family members ELOV15, ELOV13, ELOV16, and ELOV12, responsible for chain elongation of fatty acids, are strongly downregulated, e.g., CYP7B1 is downregulated by more than seven-fold in skin of *scd1*<sup>-/-</sup> mice.

### SCD1 deficiency causes downregulation of transcription factors essential for development of skin and appendages

Besides the perturbed epidermal lipid barrier function, the other remarkable tissue-specific pathological phenotypic signs of the adult *scd1*<sup>-/-</sup> skin are degenerated sebaceous glands and disturbed organogenesis of the hair follicle. To gain further insight into the molecular basis of the deletion phenotype observed, we performed a genome-wide microarray comparison of the expression

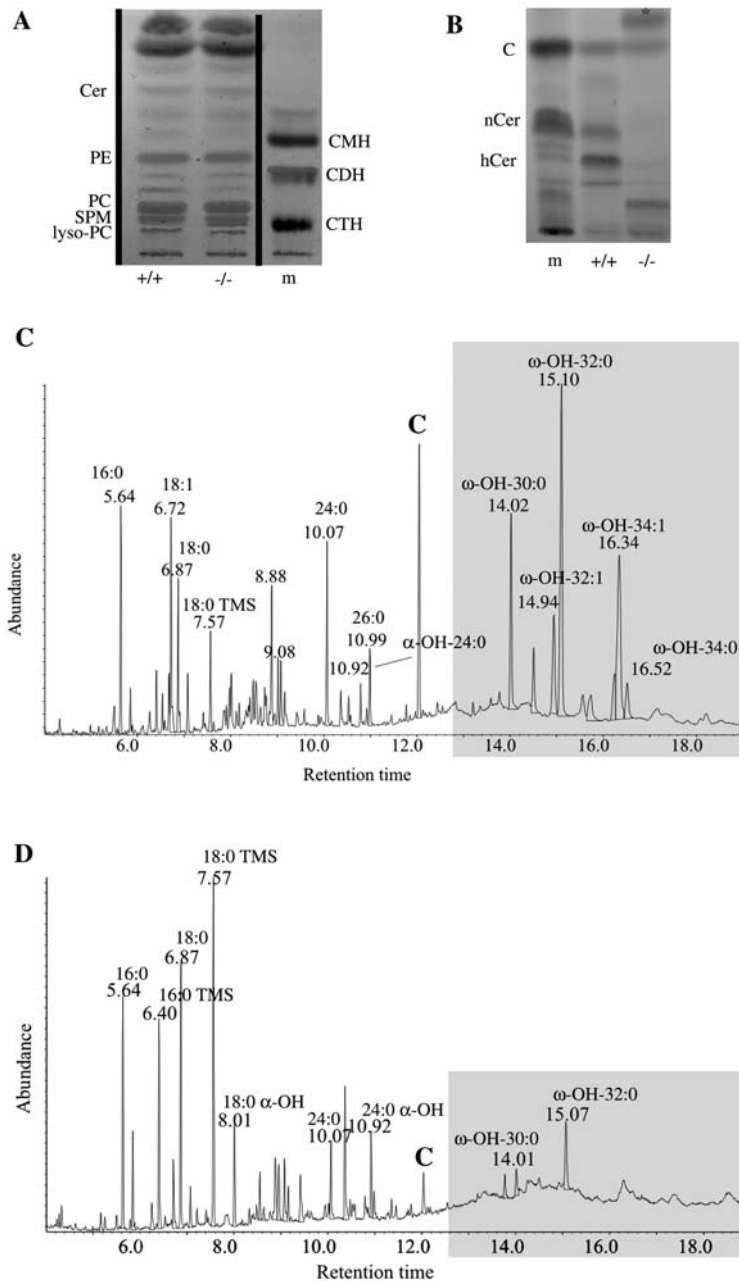


**Figure 6** Thin layer chromatographic separation of free and protein-bound epidermal lipids and GC-MS analysis of fatty acid methyl esters of the total protein-bound lipid fraction.

(A) TLC of total lipid extract of epidermis; solvent system for total lipids chloroform/methanol/2 N  $\text{NH}_4\text{OH}$  65:25:4 (by vol.). (B) Ceramides are missing in the covalently bound lipid fraction of *scd1*<sup>-/-</sup> mouse epidermis. Solvent system: chloroform/methanol/acetic acid 190:10:1 (by vol.). (C) Combined GC-MS analysis of fatty acid methyl esters of protein-bound ceramides in epidermis of p2 control (C) and *scd1*<sup>-/-</sup> mice (D).

profiles in liver and skin. The strongest regulated genes in liver and skin of the *scd1*<sup>-/-</sup> mouse are summarized in Figure 7A.

Regulators of lipid metabolism in liver were almost unchanged. In general, skin samples showed more severe perturbation of expression levels compared to liver. Particularly striking was the strong downregulation of hair keratins and associated proteins in the skin of *scd1* null mice, a possible consequence of lowered expression (11-fold) of *lef-1* (lymphoid enhancer factor 1). Lef-1 is a transcription factor required for lineage development of keratinocytes, sebocytes, and hair follicle, as well as assembly of the epidermal barrier (DasGupta and Fuchs,

1999; Niemann and Watt, 2002). Further semi-quantitative RT-PCR analysis of the steady-state mRNA level of transcription factors Lef-1 and GATA 3 at p1, p4, p11 and 3 months, and p1, p11, and 3 months, respectively (Figure 7B,C) revealed a decrease in the expression of *lef1* in the skin of *scd1*<sup>-/-</sup> mice starting at p10. In fact, *lef1* expression was almost abolished in *scd1*<sup>-/-</sup> mice aged 3 months. *gata3* expression was also reduced during this time interval by four- to six-fold (Figure 7B).

Moreover, other factors that are essential for assembly and remodeling of the extracellular matrix during embryonic development, such as Col9A3, coding type IX collagen chains, and LAMA5, an extracellular matrix laminin

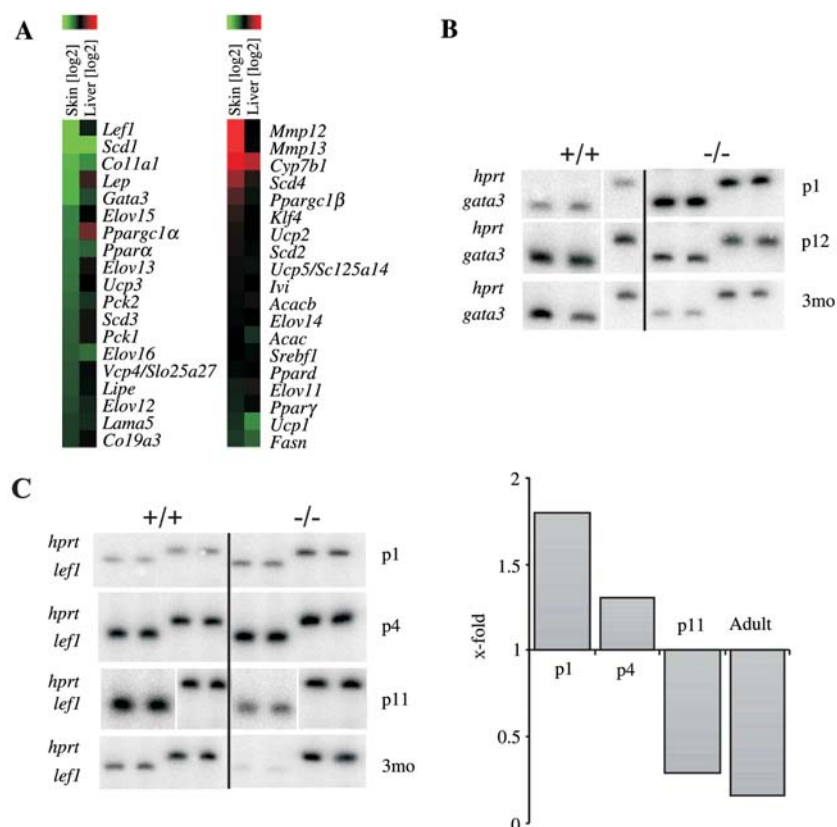


**Figure 7** Steady-state mRNA levels of genes expressed in liver and skin and genes regulating development and maintenance of sebocytes and keratinocytes in skin of control and *scd1*<sup>-/-</sup> mice. (A) Microarray analysis and assembly of genes with highest or lowest expression levels in liver and skin by semi-quantitative RT-PCR. (B) *gata3* expression decreased progressively postnatally between p1, p12, and 3 months. (C) *lef1* expression in p1, p4, p11, and 3-month *scd1*<sup>-/-</sup> mice compared with control mice.

5, showed significantly lower steady-state mRNA levels. The expression of matrix metalloproteinases 12 and 13, on the other hand, was strongly activated. Hair organogenesis of the *scd1*<sup>-/-</sup> mouse was severely altered and the hair cycle in these mice remained in telogen. The morphology of the proliferating matrix of the follicles, the resulting hair shaft, and the inner and outer root sheath were all heavily perturbed.

## Discussion

The experiments described here focused on the impact of SCD1 deficiency on hepatic metabolism and perturbation of the epidermal lipid barrier. Here, we detail aspects of the molecular basis of the complex phenotype of the SCD1-deficient mouse mutant (*scd1*<sup>-/-</sup>). The phenotype of the *scd1*<sup>-/-</sup> mutant has so far been interpreted from findings pertaining to lipid metabolic pathways of the liver leading to the hypermetabolism and obesity resistance, particularly by reduced lipid synthesis (fatty acids, triglycerides, and VLDL) in the liver (Cohen et al., 2002, 2003; Cohen and Friedman, 2004). More recently, the observation that introduction of the mutated *scd1* locus into the leptin-deficient obese (*ob/ob*) mouse genome reduced obesity led to the conclusion that *scd1* is a downstream target gene in the signal pathway of leptin, the cytokine of adipocytes (Friedman and Halaas,

1998; Cohen et al., 2002, 2003; Cohen and Friedman, 2004).

### Lipid and carbohydrate metabolism is hardly altered in the *scd1*<sup>-/-</sup> mouse

Surprisingly, SCD1 deficiency in our mouse mutant had no impact on the general pattern of non-polar and polar lipids. The pattern of phospho- and sphingolipid classes of different organs in wild-type and *scd1*<sup>-/-</sup> mice, such as liver, brain, lung, and whole blood, were similar (data not shown).

However, two remarkable differences were clearly observed among fatty acyl substituents of total lipids and of individual lipid classes for *scd1*<sup>-/-</sup> and control mice. The saturation index (16:0/16:1 and 18:0/18:1) increased from 0.8 to 2.5 in liver lipids of the *scd1*<sup>-/-</sup> mouse, but remained unchanged in brain lipids (Figure 1F). Despite SCD1 deficiency, oleic acid was still present in significant amounts in total ester (triglycerides, phospholipids, cholesterol esters, and waxes) and amide-linked lipids (ceramides, sphingomyelin, glucocerebrosides) of all tissues in the *scd1*<sup>-/-</sup> mice studied.

The other key observation was the substrate specificity of SCD1, SCD2, and SCD3 in mice. For example, palmitoleic acid ( $\Delta 9$ -16:1) was totally absent in lipid extracts of skin, liver, and brain from *scd1*<sup>-/-</sup> mice. This suggests that *de novo* synthesized palmitate is desaturated solely

by SCD1, and indicates the relative chain-length specificity of SCD1 (16:0 and 18:0), but an absolute chain-length specificity of SCD2 and SCD3 for stearoyl-CoA. Linoleic acid concentrations remained unimpaired by the SCD1 deficiency (Figure 1F).

The elevated concentration of saturated fatty acids (palmitate and stearate) in the SCD1-deficient mouse caused a dramatic reduction in VLCFA synthesis (>30 C-atoms), and particularly  $\omega$ -hydroxylated VLCFA.  $\omega$ -Hydroxylated VLCFAs are an essential acyl constituent of the epidermis-specific ceramide matrix and may be covalently linked to corneocytes and required for assembly of the epidermal lipid barrier (Abraham et al., 1985; Wertz and Downing, 1986). Taken together, our data demonstrate that breakdown of the epidermal lipid barrier plays a key role in the development of the SCD1-deficient phenotype.

The experiments described here are consistent with the hypothesis that the primary influence of SCD1 deficiency is on the epidermal lipid barrier, disruption of which leads to the complex phenotype of the mutant mouse. More specifically, the hypermetabolism present in *scd1*<sup>-/-</sup> mice is secondary. Breakdown of the epidermal lipid barrier results in uncontrolled TEWL, with heat dissipation and failure of controlled thermoregulation, elevated thermogenesis, a metabolic wasting syndrome, and fatal cold sensitivity.

#### Lack of protein-bound ceramides causes breakdown of the lipid barrier function

We focused our studies on structural defects in the epidermis and the link between skin phenotype and hypermetabolism in the *scd1*<sup>-/-</sup> mouse. Skin permeability is regulated by the lipid barrier, consisting of patterned lipid lamellae, which are deposited into the extracellular framework of cross-linked proteins in the cornified envelope between the outer granular layer (SG) and the cornified stratum (SC) (Elias and Feingold, 1988; Feingold, 1991; Elias et al., 1998).  $\omega$ -Hydroxy VLCFA-substituted ceramides esterified to residues of surface proteins of cross-linked SC play an important role in the assembly and organized packing of the epidermal lipid barrier at the SG-SC interface (Wertz and Downing, 1986).

In this study, we separated epidermis from dermis of *scd1*<sup>-/-</sup> and control p2 mice and analyzed the freely extractable sphingolipid fraction (Figure 6A), as well as the fraction containing protein-bound  $\omega$ -hydroxyceramides (Figure 6B). In *scd1*<sup>-/-</sup> epidermis,  $\omega$ -hydroxyceramides were almost absent. GC-MS analysis of the fatty acid substituents revealed that only trace amounts of VLCFA (6–8% of total fatty acids) were present in ceramides of *scd1*<sup>-/-</sup> epidermis; however, approximately two-thirds of the total fatty acid substituents of protein-bound ceramides in control epidermis were substituted with  $\omega$ -hydroxy VLCFA (Figure 6C,D).

SCD1 deficiency leads to elevated cytosolic concentrations of palmitoyl- and stearoyl-CoA, which in turn allosterically inhibit acetyl-CoA carboxylase (ACC), thereby reducing the supply of malonyl-CoA for fatty acid synthesis and microsomal chain elongation to VLCFA. VLCFAs are essential for the synthesis of epidermis-specific sphingolipids. Fatty acid chain-elongation enzyme

systems such as ELOVL1–5 that are responsible for C24–C26 VLCFA synthesis have been best described so far for yeast (Oh et al., 1997) and have paralogs in the mammalian genome. Elongases ELOV15, 13, 16 and 12 are strongly downregulated, as indicated in the microarray of skin and liver mRNA partially presented in Figure 7A. The elongase system functions in concert with the desaturase system (Stoffel, 1963; Cinti et al., 1992). No compensation by  $\omega$ -hydroxylated shorter-chain fatty acids was observed in GC-MS analysis of trimethylsilylated total fatty acid methyl esters of *scd1*<sup>-/-</sup> epidermal lipids. This suggests the presence of VLCFA (chain length)-specific  $\omega$ -hydroxylases. A skin-specific elongase, ELOVL3, has been described in the mouse (Westerberg et al., 2004). Disruption of the *elov3* gene by homologous recombination in mouse proved its participation in the formation of specific neutral lipids and requirement for skin function.

Our biochemical data were supported by gene expression data obtained from microarrays. Expression of elongases *elov15*, *13*, *16*, and *12* were strongly downregulated in skin, as well as *elov16* in skin and liver, of SCD1-deficient mice. In addition, expression of *cyp7B1*, coding for a lipid hydroxylase, was strongly reduced. Future studies will address regulation of the elongase and hydroxylase systems in epidermal VLCFA synthesis.

Taken together, these observations lead to the conclusion that the lack of covalently linked ceramide brush-border-like matrix for assembly of the epidermal lipid multilayer barrier is the structural basis of the complex SCD1-deficient phenotype.

UVB irradiation and feeding an essential fatty acid-deficient (EFAD) diet to hairless rats led a significantly lower amount of covalently bound ceramides in the SC and significant elevation of TEWL, indicating impairment of the epidermal barrier function (Meguro et al., 2000).

Recently, an *scd2*-null mouse mutant has been described (Miyazaki et al., 2005). Most of the newborn homozygous mice died within 24 h after birth, presumably because of dehydration, different from the *scd1*<sup>-/-</sup> mouse, which has a normal postnatal life span. The epidermal barrier defect and associated water loss of the *scd2* mouse has been interpreted as a reduced level of epidermal acylglucosylceramides, acylceramides and linoleic acid-substituted acylceramides. A shift of linoleic acid into the phospholipid fraction at the expense of the acylceramide fraction has been suggested to mimic the barrier defect in essential fatty acid deficiency. The liver or epidermis-specific rescue of SCD1 deficiency will further our insight into the protein-bound, VLCFA (<28 C)-substituted, ceramide layer of the *scd1*<sup>-/-</sup> mouse, which is essential for regulated epidermal barrier function and the overall phenotype of the *scd1*<sup>-/-</sup> mutant described here.

#### Dysfunction of the epidermal lipid barrier and energy metabolism

Perturbation of the epidermal lipid barrier causes uncontrolled high TEWL (Figure 3A) associated with elevated heat dissipation in *scd1*<sup>-/-</sup> mice (Figure 3D), even when housed at ambient temperature of 23°C (7°C below thermoneutrality). We showed that core body temperature in

the *scd1*<sup>-/-</sup> mutant was maintained by elevated thermogenesis via uncoupling of oxidative phosphorylation, mainly in muscle, which follows the elevated cytosolic concentration of palmitate and stearate (Figure 4B–D) known to uncouple mitochondrial oxidative phosphorylation.

Gene expression analysis by semi-quantitative RT-PCR revealed remarkable changes in key regulators of adaptive thermoregulation in muscle and adipose tissue (Figure 4A–D). The overexpression of *ucp1*, *ucp2*, and *ucp3* in muscle suggests that muscle is the target tissue for efferent sympathetic signaling in *scd1*<sup>-/-</sup> mice (Figure 4A,B). *ucp1* expression was strongly enhanced (16-fold) only in skeletal muscle to compensate for the increased energy expenditure due to overall heat loss. In BAT of *scd1*<sup>-/-</sup> mice, *ucp1* and *ucp3* expression was almost absent (Figure 4C,D). Steady-state levels of *pgc1α* and *pgc1β* mRNA, the coactivator of PPAR $\gamma$  of *ucp1* and other promoters of genes involved in thermogenesis, remained unchanged in BAT and muscle of *scd1* mutants.

Sympathetic signals activate catecholamine-sensitive lipase, which mobilizes the triglyceride stores of target tissues (BAT and WAT) for energy production via mitochondrial  $\beta$ -oxidation of predominantly palmitate and stearate in muscle. Consequently, *scd1*<sup>-/-</sup> mice progressively lose their fat stores.

Substantial support of the causal sequence proposed here for the development of the hypermetabolic phenotype of *scd1* null mice came from two experiments: cold-induced stress experiments and rescue of the barrier function by artificial occlusion of the skin by topical application of a paraffin (Vaseline) coat (Figure 5A–F).

We challenged adaptive thermogenesis in our *scd1*<sup>-/-</sup> mouse by cold exposure. Cohorts of *scd1*<sup>-/-</sup> mice with free access to food and water showed a complete loss of adaptive thermoregulation within short periods of cold exposure. Their core body temperature dropped by 10°C

within 1–3 h (Figure 5F), and all succumbed within 4 h at 4°C. Control mice with free food and water access, however, survived the 24-h experiment at 4°C without a significant change in body temperature. The core body temperature of fasting *scd1*<sup>-/-</sup> mice dropped by 10°C within 1–1.5 h, whereas in control mice this was not observed before 4 h (Figure 5F). This suggests that the energy supply in the mutant, unlike in the wild-type mouse, is insufficient to cope with heat loss through the disturbed epidermis lipid barrier.

Blood glucose levels of *scd1*<sup>-/-</sup> mice fell during cold stress to <60–70 mg/dl. During this experiment, *ucp1* expression in *scd1* mutant mice was shut off, despite induction of *pgc1* expression in adipose tissue and skeletal muscle by seven- and 3.5-fold, respectively. Energy supply either via fatty acid  $\beta$ -oxidation or glucose oxidation generated by increased gluconeogenesis was not sufficient for the survival of *scd1*<sup>-/-</sup> mice.

Figure 8 summarizes the proposed molecular links between SCD deficiency, structural defects, and dysfunction of the epidermal lipid barrier and the metabolic wasting syndrome.

If our proposal that the epidermal lipid barrier defect is the ultimate link from the enormous TEWL and heat of evaporation to the compensatory hypermetabolism and disrupted thermogenesis, then a topically applied artificial paraffin coat should improve or recover the parameters of TEWL and quantitative calorimetry, as well as the survival rate in cold stress experiments. This was indeed observed within 12–24 h after occlusion of the skin of *scd1*<sup>-/-</sup> mice (Figure 5A), with TEWL for coated *scd1*<sup>-/-</sup> mice reduced by approximately 50% compared to the control. Furthermore, O<sub>2</sub> consumption, CO<sub>2</sub> production and heat dissipation dramatically changed (Figure 5B–D). Finally, the core body temperature of paraffin-coated mutant mice resisted the rapid drop observed in untreated *scd1*<sup>-/-</sup> mice during cold stress at 4°C (Figure 5F).

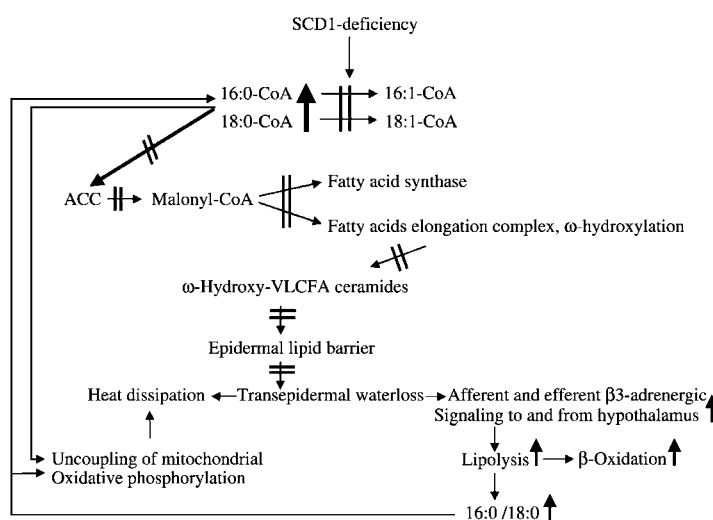


**Figure 8** Molecular links between stearoyl-CoA desaturase deficiency and dysfunctions of the epidermal lipid barrier.

The elevated concentration of saturated long-chain fatty acids allosterically inhibits acetyl-CoA carboxylase (ACC), which causes reduced malonyl-CoA concentrations and consequently *de novo* fatty acid synthesis and chain elongation, and reduced epidermal synthesis of  $\omega$ -hydroxy-VLCFA, which are essential substituents of sphingolipids of the epidermal lipid barrier. The breakdown of the barrier causes water loss, heat dissipation and disruption of thermoregulation.

### The lipid barrier in *scd1*<sup>-/-</sup> mice in relation to human ichthyoses and atopic dermatitis

Similar to *scd1*<sup>-/-</sup> mice, an impaired epidermal permeability barrier has been described in many human ichthyoses. Ichthyosis in children is associated with increased TEWL and a caloric drain through heat of evaporation. This chronic energy expenditure is associated with growth failure.

The missing protein-bound  $\omega$ -hydroxyceramide layer in the epidermal lipid barrier in *scd1*<sup>-/-</sup> mice associated with severely impaired permeability of the epidermal barrier, as described above, might be linked to the pathobiochemistry of atopic dermatitis, a common skin disease of unknown etiology in humans. Protein-bound  $\omega$ -hydroxyceramides in the epidermis of atopic dermatitis subjects are reduced to approximately half the amount observed for healthy epidermis (23–28% vs. 46–53%) in non-lesional areas, and even less in affected atopic skin areas (10–25%) (Macheleidt et al., 2002). The occurrence of SCD1 and the newly described hSCD5 (ACOD4) in humans suggests that the *scd1*<sup>-/-</sup> mouse mutant might be a valuable animal model for the study of human skin diseases associated with epidermal barrier defects.

### Is SCD1 involved in signal transduction of keratinocytes and sebocytes?

A particularly striking feature of *scd1*<sup>-/-</sup> mice is the virtual absence of functional hair follicles and sebaceous glands, which might be a consequence of *lef1* downregulation. It is currently not clear, however, how this phenotype is coupled to the deficiency of unsaturated fatty acids. A possible link is offered by the observation that efficient Wnt signaling, a major upstream regulator of Lef-1 levels, requires fatty acid modification of secreted Wnt proteins to target them to the appropriate lipid rafts (Wilfert et al., 2003; Zhai et al., 2004). Therefore, it is conceivable that lipid perturbations caused by *scd1* deletion can interfere with this targeting process.

Sebocytes, which strongly express *scd1*, as demonstrated by *in situ* hybridization, are lost in the *scd1*<sup>-/-</sup> mouse (Miyazaki et al., 2001). Sebaceous glands develop in *scd1*<sup>-/-</sup> newborns within the first postnatal days. By p11, they begin to become atrophic and are visible only as rudimentary structures after the first 3–6 weeks. Differentiation and maintenance of sebaceous glands is regulated by the transcription factor Lef-1. It was observed that steady-state mRNA levels of *lef1* in the epidermis of *scd1*<sup>-/-</sup> mice rapidly decreased postnatally within 4 weeks, in parallel to the onset of morphological changes (Figure 7C). This observation raises the question as to whether the increase in saturation index and/or the absence of palmitoleate in *scd1*<sup>-/-</sup> mice causes downregulation of the transcriptional activity of *lef1* or whether this is a secondary event. Future studies will address the role of palmitoleic acid as a potential ligand of transcription factors, as well as *lef1*-induced signaling, in keratinocyte, hair, and sebocyte development in SCD1 deficiency.

GATA 3 is another essential regulator of developmental processes of keratinocytes, sebocytes, and hair follicles

(Zheng et al., 1999). *gata3* expression appeared to be highly downregulated in microarray analysis and quantitative RT-PCR in *scd1*<sup>-/-</sup> skin (Figure 7B).

We found that the hair cycle of *scd1*<sup>-/-</sup> mice remained in telogen. Our data suggest that SCD1 deficiency restrains the hair shaft from growing out of the follicle. The cleft between the hair shaft and sheath appears obliterated and slipping of the hair shaft out of the sheath was inhibited, with reversed growth. In p6 mutant mice, follicles emerged, pouching out into the dermis, and at p40, follicular dystrophy was observed (data not shown).

Remodelling processes in the skin of *scd1*<sup>-/-</sup> mice are further indicated by reduced expression of Col9A3, essential for the assembly of type IX collagen molecules and LAMA5 (laminin5 $\alpha$ ), a mediator of attachment, migration, and organization of cells into tissues during embryonic development, as well as by strong activation of matrix metalloproteinases MMP 12 and 13 expression (Figure 7A).

Taken together, our observations necessitate a rethinking of previous interpretations of the *scd1* null mouse model, and future experiments will be necessary to define the link between SCD1 and remodeling processes of the developing epidermis.

### Materials and methods

1-[<sup>14</sup>C]Palmitoyl-CoA was purchased from Amersham (Braunschweig, Germany), 1-[<sup>14</sup>C]stearoyl-CoA from Biotrend Chemicals (Cologne, Germany), and palmitoyl-CoA and stearoyl-CoA were obtained from Sigma-Aldrich (Taufkirchen, Germany).

Mice were housed at 23°C under a 12 h/12 h light/dark cycle, and fed *ad libitum* a standard laboratory chow diet (Altromin 1314) or a fat-depleted diet (C 1056, Altromin, Lage, Germany).

### Generation of the *scd1*<sup>-/-</sup> mouse

Genomic DNA of CJ7 cells containing exons I–IV (approx. 7 kb) of the *scd1* gene was amplified with primers for the *sXhoI* end of exon 1 (5'-TCC CAG TCT CGA GGG GTT TCT CTT TGC TGG-3') and the *KpnI* end of exon 4 (5'-CTC CCA TGG AAC ATC ACC AGC TTC TCG GCT-3') and subcloned into the pCR2.1 vector for sequencing and restriction enzyme analysis. The 3' 5-kb fragment was obtained by PCR using primers for the *sBamHI* end of exon 2 (5'-CGG GAT CAT ACT GGA TCC CTC CTG CAA GCT-3') and the *asBamHI* end of exon 4 (5'-CAC CAG CTT CTC GGA TCC CAG GTC AGA CAT), which contained several stop codons introduced into the pCR2.1 vector. The insert was then excised as a *SpeI/NotI* fragment and ligated blunt-ended into the *BamHI* site of pPNT. The orientation was determined by *KpnI* restriction. A 1.8-kb fragment that encoded exons I and II flanked by *XhoI* restriction sites was amplified with the above 5' *XhoI* primer and primer for the delta 9 *XhoI* end of exon II (5'-GCT CAC CGA AGA GGG CAG TCT CGA GCT TGC-3'), then inserted into the *XhoI* site of the pPNT vector. The orientation was determined by *BamHI/NotI* restriction to yield the *scd1* construct pPNT 5'-ex1-2/3' ex2-4scd1. The selection markers *neo* and *tk* were under the control of the *pgk* promoter.

The targeting vector was linearized with *NotI* for electroporation of ES cells (CJ7). A 1.2-kb *SpeI* fragment obtained by PCR using a 5' external sense oligonucleotide for exon 4 delta9 *Bam*s (5'-AGC CGA GAA GCT GGT GAG GAT CCA GAG GAG-3') and exon 5 delta 9 *Bam* (5'-CAC GGC ACC CAG GGA TCC CAG

GAT ATT CTC-3') served as an external probe in genotyping for the homologous recombination event in ES cell clones and tail DNA of mice by Southern blot hybridization (Figure 1). The wild-type genomic sequence yielded a 6.5-kb fragment, while the homologous recombination event was indicated by an 8-kb fragment. Conditions for PCR of genomic DNA were 2 min at 94°C, 30 s at 60°C and 7 min at 68°C for 30 cycles. ES cell clones with the targeted *scd1* locus were injected into blastocysts and implanted into CD1 foster mothers. Germline chimeric males were crossed to homozygosity with C57BL/6J females.

### Gene expression analysis

Total RNA was extracted from tissues of 6-week-old wild-type mice and *scd1*<sup>-/-</sup> mutants using Trizol reagent according to the manufacturer's instructions (Gibco-BRL, Karlsruhe, Germany). DNaseI treatment (25 U/10 µg) of total RNA removed contaminating genomic DNA. For semi-quantitative analysis of expression levels, cDNA was synthesized using Maloney murine leukemia virus reverse transcriptase, random hexamer primers, and dNTPs. cDNA templates were amplified by PCR with specific primers in the presence of dNTPs, [ $\alpha$ -<sup>32</sup>P] dCTP, and Taq polymerase, using 19 cycles of 2 min at 94°C, 1 min at 93°C, 1 min at 60°C and 2.5 min at 72°C, ending with one cycle for 10 min at 72°C. Primer sequences are available on request.

### Microarray experiments

Samples of 1 µg of total RNA were used for cDNA synthesis with a LOW RNA Input Linear Amp Kit (Agilent Technologies, Waldbronn, Germany). Half of the reaction mixture was subsequently used for complementary RNA (cRNA) synthesis and fluorescent labeling according to the manufacturer's protocol. Hybridization was performed according to the Agilent 60-mer oligo microarray processing protocol for Whole Mouse Genome Oligo Microarrays (44K) using the hybridization chamber and oven recommended by Agilent. The resulting raw data sets derived from dye swap experiments for skin and liver samples were combined using the Luminator software. Genes differentially expressed in tissues of wild-type and null mice were selected using conservative filter criteria ( $p < 0.0001$ , >two-fold change).

cDNAs were also hybridized to the metabolic, skin, cell signaling, and cytokine-onco microarrays (12 000 genes; MEMOREC Biotec, Cologne, Germany) according to the manufacturers protocol. Hybridization data were analyzed using the MEMOREC software. The algorithm ranked genes based on the extent to which expression was decreased or enhanced in homozygous compared to wild-type mice and these were averaged to give the score of expression for each gene. The primer sequences used are available on request.

### Enzyme assay

Mouse liver was homogenized in 0.25 M sucrose at 4°C and centrifuged at 10 000 g. The supernatant of the postmitochondrial fraction (10 000 g, 10 min) was sedimented at 100 000 g for 1 h and yielded the microsomal fraction and supernatant.

For assay of stearoyl-CoA desaturase, a reaction volume of 100 µl of 0.1 M Tris buffer, pH 7.4 contained 10 µM 1-[<sup>14</sup>C] stearoyl-CoA (200 000 dpm), 5 mM NADH, 1 mM ATP and 50–100 µg of microsomal protein, which was incubated for 30 min at 37°C. An equal volume of 0.5 M KOH-methanol was added to the reaction mixture, which was incubated for 1 h at 37°C and acidified with 2 N HCl. Free fatty acids were then extracted with hexane/ether 1:1 (v/v). The solvent was evaporated and the fatty acids were esterified with 5% HCl-methanol for 1 h at 80°C. Then 0.5 ml of water was added and the fatty acid methyl esters were

extracted with hexane and concentrated for GC analysis and for TLC separation on 10% silver nitrate-impregnated silica gel plates using hexane/ethyl ether 9:1 (v/v) as solvent. Radioactive bands were visualized and quantified in a phosphorimager using ImageQuant software.

### Isolation, fractionation, and identification of lipids

Total lipids were extracted from liver, brain, kidney, and muscle. Tissues were homogenized in an Ultraturax in 10 volumes of chloroform/methanol (C/M, 2:1 v/v) and re-extracted using C/M 1:1 (v/v) and then C/M 1:2 (v/v) for 2 h at 37°C under a stream of nitrogen. The combined extracts were dissolved in C/M 2:1 (v/v), washed with 2 M KCl, and concentrated.

Skin was powdered under liquid nitrogen in a mortar prior to extraction. Total lipids were extracted from skin or epidermis as described above.

Lipids were separated on 0.25-mm silica gel G plates in the following solvent systems: neutral lipids, hexane/ethyl ether/acetone 70:30:1 (by vol.); ceramide fraction, C/M/AcOH 190:10:1 (by vol.) and chloroform/methanol 15:1 (v/v); complex lipids, C/M/2 N NH<sub>4</sub>OH 65:25:4 (by vol.). For fatty acid analysis, lipid bands were visualized with 2,7-dichlorofluorescein (5 mM) in ethanol, collected on small fitted glass filters, and eluted with C/M 2:1 (v/v).

Ester lipids were saponified in 0.5 N KOH in methanol for 2 h at 40°C. Unsaponifiable lipids were extracted with dichloromethane, the aqueous phase was acidified with 2 N HCl, fatty acids were extracted with hexane/ether 1:1 (v/v), concentrated, and then esterified with 5% HCl-methanol at 80°C for 2 h under reflux. One volume of water was added and the fatty acid methyl esters were extracted with hexane for GC-MS and GC analysis.

### Gas chromatography-mass spectrometry (GC-MS)

Combined gas liquid chromatography electrospray ionization tandem mass spectrometry (ESI-MS/MS) of TMS-derivatized fatty acid methyl esters and sphingosine bases was performed on an Agilent 6890/5973N instrument equipped with a HP-5MS fused silica column (length, 17 m; i.d., 0.25 mm; film thickness, 0.25 µm). TMS-derivatized samples (2 µl) were injected with a split ratio of 10:1 into the mass spectrometer, which was operated in full scan mode over a mass range of 50–500 u, and electron ionization (EI) was utilized at 70 eV. The injector temperature was set to 300°C.

ESI-MS/MS was performed on an Applied Biosystems (Darmstadt, Germany) QTrap analyzer. Analytes were dissolved in methanol containing 5 mM ammonium acetate and introduced into the ion source via a Hamilton syringe pump at 3 µl/min. The ESI source was operated at room temperature using a spray voltage of 5500 V. Sheath and collision gas was nitrogen delivered from a Peak Scientific (Inchinnan, Scotland) MN30L nitrogen generator. Declustering and collision offset potentials were adjusted to 50 V in precursor and product ion scan experiments. The collision gas pressure was 4.0×10<sup>-3</sup> Pa during precursor ion scanning in the triple quadrupole mode and 5.3×10<sup>-3</sup> Pa during product ion scanning in the linear ion trap mode. Mass ranges of 200–750 u and 50–700 u, respectively, were recorded.

### Northern blot hybridization analysis

Total RNA was extracted following the Trizol protocol. RNA (25 µg) from the organs listed was separated by 1% agarose-formaldehyde gel electrophoresis and transferred to a nylon membrane. The membranes were hybridized with [<sup>32</sup>P]-labeled *scd1*, *scd2*, and *scd3* cDNA probes. A *gapdh* cDNA probe was used as a loading control.

## Separation of epidermis from dermis

The epidermis of wild-type and homozygous *scd1*<sup>-/-</sup> p1 and p2 littermates was isolated by floating the skin on 0.025% trypsin and 1 mM EDTA with the epidermis side up at 4°C overnight. The epidermis was then peeled from the dermis using forceps.

## Histology

Mice were perfused from the left ventricle with the right atrium opened with saline, followed by 4% buffered paraformaldehyde. Tissues were fixed in 4% paraformaldehyde and embedded in paraffin or OTEC for cryosections.

## Blood plasma and serum analytes

Leptin concentrations were measured in plasma from control and *scd1*<sup>-/-</sup> mice at the time points indicated using a commercially available mouse leptin ELISA kit (Crystal Chem. Inc, Minneapolis, USA). Plasma glucose, serum triglycerides, VLDL, LDL, and total cholesterol were measured in the same samples using a Modula Instrument (Roche, Mannheim, Germany).

## Quantification of transepidermal water loss (TEWL)

TEWL of age- and sex-matched cohorts of 10 wild-type and *scd1*<sup>-/-</sup> mice each was examined at 22°C ambient temperature and 55–60% humidity using a model 210 Courage-Khazaka Tewameter (Courage-Khazaka, Cologne, Germany). The manufacturer's software was used to determine the parameters. Humidity and temperature sensors measured water evaporation at the dorsal skin surface of neonatal, developing, and adult wild-type and *scd1*<sup>-/-</sup> mutants.

## In vitro [<sup>3</sup>H]-mannitol diffusion

To separate the outside (receiver) and inside (donor) compartments (volume 1.5 ml), the dorsal skin of mice was excised and mounted in a diffusion chamber filled with PBS, pH 7.4. The effective skin surface was 1.75 cm<sup>2</sup>. The system was equilibrated at room temperature for 30 min. [<sup>3</sup>H]-Mannitol was added to the donor compartment and 200-μl aliquots were taken from the receiver compartment of wild-type and *scd1*<sup>-/-</sup> mice for radioactivity measurements at the intervals indicated. The aliquots removed were replaced with 200 μl of fresh PBS.

## Transdermal permeation of Lucifer yellow in vivo

The functionality of the epidermal permeation barrier of age- and gender-matched *scd1*<sup>-/-</sup> and control littermates was compared *in vivo*. Anesthetized mice were placed with their back in a cone-shaped vessel filled with 1 mM Lucifer yellow in PBS, pH 7.4 at 30°C for 1 h. Mice were sacrificed and the dorsal skin was excised and embedded for cryosectioning, with 5–8-μm thick sections used for epifluorescence microscopy.

## Acknowledgments

These studies were funded by the Center of Molecular Medicine Cologne (CMMC), University of Cologne, Germany. Clinical chemistry was kindly carried out by Prof. Dr. K. Wielckens, Institute of Clinical Chemistry, University of Cologne. Experiments were carried out in accordance with the guidelines of the Ethics Committee of the Faculty of Medicine, University of Cologne.

## References

- Abraham, W., Wertz, P.W., and Downing, D.T. (1985). Linoleate-rich acylglucosylceramides of pig epidermis: structure determination by proton magnetic resonance. *J. Lipid Res.* 26, 761–766.
- Cinti, D.L., Cook, L., Nagi, M.N., and Suneja, S.K. (1992). The fatty acid chain elongation system of mammalian endoplasmic reticulum. *Prog. Lipid Res.* 31, 1–51.
- Cohen, P. and Friedman, J.M. (2004). Leptin and the control of metabolism: role for stearoyl-CoA desaturase-1 (SCD-1). *J. Nutr.* 134, 2455–2463.
- Cohen, P., Miyazaki, M., Socci, N.D., Hagge-Greenberg, A., Liedtke, W., Soukas, A.A., Sharma, R., Hudgins, L.C., Ntambi, J.M., and Friedman, J.M. (2002). Role for stearoyl-CoA desaturase-1 in leptin-mediated weight loss. *Science* 297, 240–243.
- Cohen, P., Ntambi, J.M., and Friedman, J.M. (2003). Stearoyl-CoA desaturase-1 and the metabolic syndrome. *Curr. Drug Targets Immune Endocr. Metab. Disord.* 3, 271–280.
- DasGupta, R. and Fuchs, E. (1999). Multiple roles for activated LEF/TCF transcription complexes during hair follicle development and differentiation. *Development* 126, 4557–4568.
- Dobrzyn, A. and Ntambi, J.M. (2005). The role of stearoyl-CoA desaturase in the control of metabolism. *Prostaglandins Leukot. Essent. Fatty Acids* 73, 35–41.
- Elias, P.M. and Feingold, K.R. (1988). Lipid-related barriers and gradients in the epidermis. *Ann. NY Acad. Sci.* 548, 4–13.
- Elias, P.M., Cullander, C., Mauro, T., Rassner, U., Komuves, L., Brown, B.E., and Menon, G.K. (1998). The secretory granular cell: the outermost granular cell as a specialized secretory cell. *J. Invest. Dermatol. Symp. Proc.* 3, 87–100.
- Feingold, K.R. (1991). The regulation of epidermal lipid synthesis by permeability barrier requirements. *Crit. Rev. Ther. Drug Carrier Syst.* 8, 193–210.
- Friedman, J.M. and Halaas, J.L. (1998). Leptin and the regulation of body weight in mammals. *Nature* 395, 763–770.
- Kaestner, K.H., Ntambi, J.M., Kelly, T.J. Jr., and Lane, M.D. (1989). Differentiation-induced gene expression in 3T3-L1 preadipocytes. A second differentially expressed gene encoding stearoyl-CoA desaturase. *J. Biol. Chem.* 264, 14755–14761.
- Macheleidt, O., Kaiser, H.W., and Sandhoff, K. (2002). Deficiency of epidermal protein-bound omega-hydroxyceramides in atopic dermatitis. *J. Invest. Dermatol.* 119, 166–173.
- Meguro, S., Arai, Y., Masukawa, Y., Uie, K., and Tokimitsu, I. (2000). Relationship between covalently bound ceramides and transepidermal water loss (TEWL). *Arch. Dermatol. Res.* 292, 463–468.
- Miyazaki, M., Man, W.C., and Ntambi, J.M. (2001). Targeted disruption of stearoyl-CoA desaturase 1 gene in mice causes atrophy of sebaceous and meibomian glands and depletion of wax esters in the eyelid. *J. Nutr.* 131, 2260–2268.
- Miyazaki, M., Jacobson, M.J., Man, W.C., Cohen, P., Asilmaz, E., Friedman, J.M., and Ntambi, J.M. (2003). Identification and characterization of murine SCD4, a novel heart-specific stearoyl-CoA desaturase isoform regulated by leptin and dietary factors. *J. Biol. Chem.* 278, 33904–33911.
- Miyazaki, M., Dobrzyn, A., Elias, P.M., and Ntambi, J.M. (2005). Stearoyl-CoA desaturase-2 gene expression is required for lipid synthesis during early skin and liver development. *Proc. Natl. Acad. Sci. USA* 102, 12501–12506.
- Niemann, C. and Watt, F.M. (2002). Designer skin: lineage commitment in postnatal epidermis. *Trends Cell Biol.* 12, 185–192.
- Ntambi, J.M., Miyazaki, M., and Dobrzyn, A. (2004). Regulation of stearoyl-CoA desaturase expression. *Lipids* 39, 1061–1065.
- Oh, C.S., Toke, D.A., Mandala, S., and Martin, C.E. (1997). *ELO2* and *ELO3*, homologues of the *Saccharomyces cerevisiae ELO1* gene, function in fatty acid elongation and are required for sphingolipid formation. *J. Biol. Chem.* 272, 17376–17384.

- Puigserver, P., Wu, Z., Park, C.W., Graves, R., Wright, M., and Spiegelman, B.M. (1998). A cold-inducible coactivator of nuclear receptors linked to adaptive thermogenesis. *Cell* 92, 829–839.
- Stoffel, W. (1963). Stoffwechsel der ungesättigten Fettsäuren, I. Zur Biosynthese hochungesättigter Fettsäuren. *Hoppe-Seyler's Z. Physiol. Chem.* 333, 71–88.
- Sundberg, J.P., Boggess, D., Sundberg, B.A., Eilertsen, K., Parimoo, S., Filippi, M., and Stenn, K. (2000). *Asebia-2J* [*Scd1(ab2J)*]: a new allele and a model for scarring alopecia. *Am. J. Pathol.* 156, 2067–2075.
- Wertz, P.W. and Downing, D.T. (1986). Covalent attachment of omega-hydroxyacid derivatives to epidermal macromolecules: a preliminary characterization. *Biochem. Biophys. Res. Commun.* 137, 992–997.
- Westerberg, R., Tvrdik, P., Uden, A.B., Mansson, J.E., Norlen, L., Jakobsson, A., Holleran, W.H., Elias, P.M., Asadi, A., and Flodby, P., et al. (2004). Role for ELOVL3 and fatty acid chain length in development of hair and skin function. *J. Biol. Chem.* 279, 5621–5629.
- Willert, K., Brown, J.D., Danenberg, E., Duncan, A.W., Weissman, I.L., Reya, T., Yates, J.R. III, and Nusse, R. (2003). Wnt proteins are lipid-modified and can act as stem cell growth factors. *Nature* 423, 448–452.
- Zhai, L., Chaturvedi, D., and Cumberledge, S. (2004). *Drosophila wnt-1* undergoes a hydrophobic modification and is targeted to lipid rafts, a process that requires porcupine. *J. Biol. Chem.* 279, 33220–33227.
- Zheng, Y., Eilertsen, K.J., Ge, L., Zhang, L., Sundberg, J.P., Proudy, S.M., Stenn, K.S., and Parimoo, S. (1999). *Scd1* is expressed in sebaceous glands and is disrupted in the *asebia* mouse. *Nat. Genet.* 23, 268–270.

Received October 17, 2006; accepted January 18, 2007